Powder Contamination during Laser Powder Bed Fusion: Inconel 718 in Ti6Al4V

Cory Groden, Kellen D. Traxel, and Amit Bandyopadhyay*

W. M. Keck Biomedical Materials Research Lab
School of Mechanical and Materials Engineering
Washington State University, Pullman, WA 99164, USA.
*Corresponding author email: amitband@wsu.edu

Abstract

Powder contamination during laser powder bed fusion is a critical concern for the quality assurance of parts. Herein, we studied the effect of Inconel 718 contamination on the properties of printed Ti6Al4V, two commonly printed alloys. Contaminated parts exhibited visual and microstructural defects, and a mere 0.5wt% IN718 contamination resulted in a 43% reduction in plastic strain without noticing surface-level cracking. Further contamination of 2.5 wt% IN718 promotes surface cracking that renders the material unable to deform plastically, highlighting the importance of proper powder handling and the detrimental effects that even small amounts of contaminants can have on AM-produced components.

Keywords*:* Laser powder bed fusion; Additive Manufacturing; Inconel 718; Ti6Al4V; Defects; Mechanical Properties.

1. Introduction

One key drawback to metal additive manufacturing (AM) is the defects that can form during the process, such as keyhole or gas-based porosity, residual stress, delamination, foreign particle inclusions, mechanical property anisotropy, microcracking, among others [1-8]. The high volume of powder needed to produce parts can add to these defects due to contamination concerns in manufacturing environments. There are several ways that this can occur, beginning with powder preparation or machine loading and going all the way through to building cleaning, where concealed powder in blind spots can remain. This is particularly problematic if the same tools or printers are used for processing different materials in the

same machine. Some studies have found that powder contamination can decrease the mechanical properties of the AM processed material, including Ti contamination in maraging steel, which caused decreased fatigue life [9], and the presence of W particles in Ti6Al4V resulted in a reduction in elongation [10]. Because of this, understanding the influence of these contaminants on the material properties of as-printed parts is of the utmost importance and remains largely unexplored.

Ti6Al4V is a popular 3D-printed alloy in the aerospace and biomedical industries due to its high strength, low density, and excellent corrosion and fatigue resistance [11-14]. Inconel 718 (IN718) is a nickel-based superalloy commonly printed for aerospace applications due to its excellent strength retention at high temperatures [15-16]. Since manufacturers regularly use both compositions in laser-based PBF, potential contamination during machine material changes is possible. The contamination of Ti6Al4V with IN718 is particularly problematic because Ti and Ni react to form brittle intermetallic compounds such as Ti_2Ni and $TiNi_3$, which have been observed during laser welding [17, 18], and during AM of composite bimetallic and graded structures [19-21]. To measure the extent of these detrimental effects on part quality and performance in L-PBF, batches of Ti6Al4V samples were printed with various amounts of IN718 contamination. Subsequently, multiple parts with simple and complex geometries were created to observe visible cracking/defects and were analyzed using scanning electron microscopy (SEM), energy dispersive spectroscopy (EDS), and X-ray diffraction (XRD), followed by mechanical testing. Our results help manufacturers understand the extent to which contamination during PBF can influence the properties of their resulting parts.

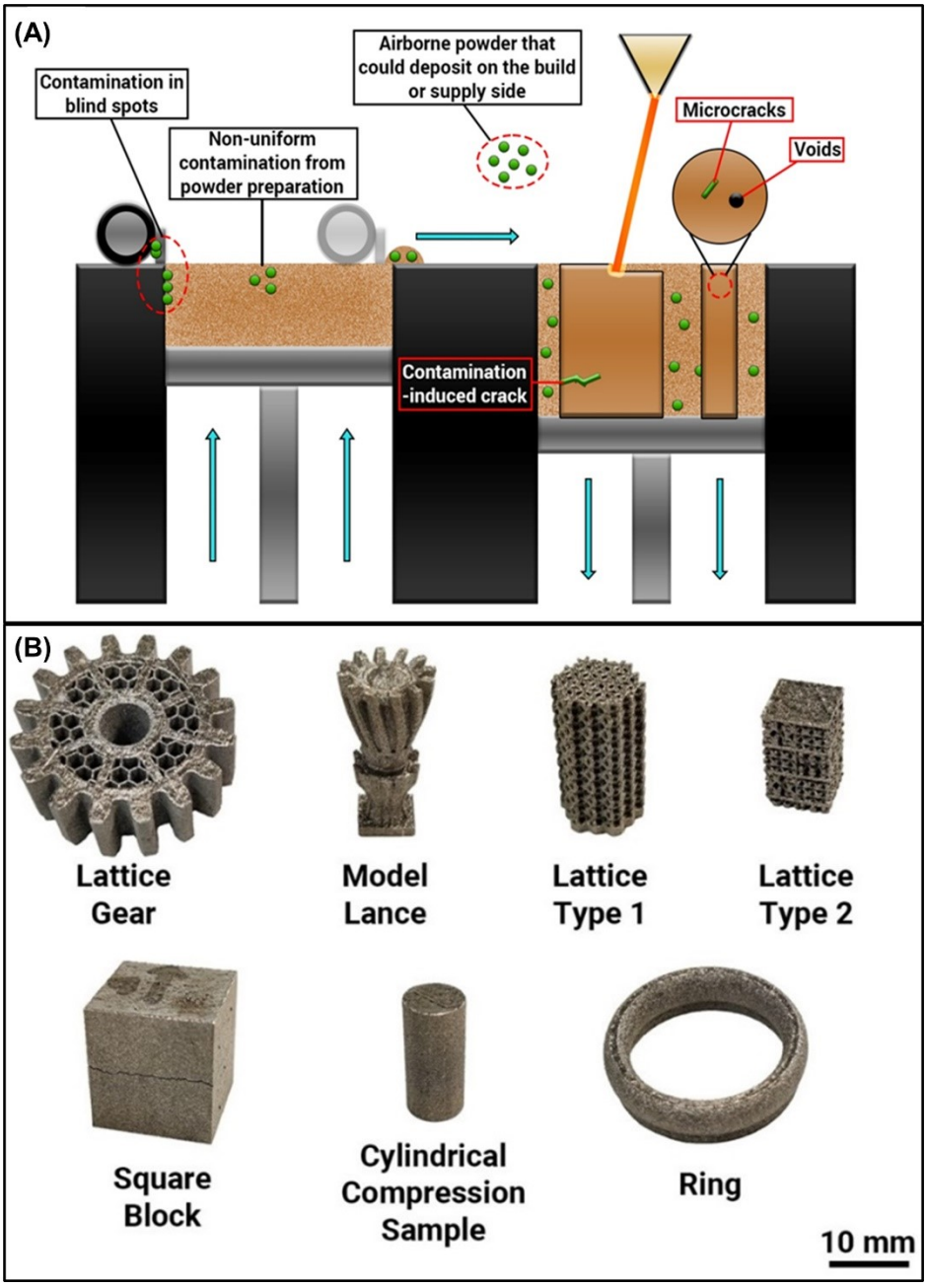

Figure 1: The experimental setup of the laser powder bed fusion shows (A) regions of the build chamber that may experience contaminants and (B) designed components printed with contaminants.

2. Materials and Methods

All samples were fabricated using a 3D Systems Powder Bed Fusion AM printer (ProX DMP 200, Rock Hill, SC, USA). IN718 powder (Powder Alloy Corporation, OH, USA) and

Grade-5 Ti6Al4V powder (3D Systems, SC, USA) were sieved to 15-45µm, mixed in the prescribed weight proportion, and milled (without milling media) for 1h prior to printing to ensure compositional homogeneity prior to deposition. Four different sets of samples were printed, which included pure Ti6Al4V, Ti6Al4V + 0.5% IN718 (INC0.5), Ti6Al4V + 1.5% IN718 (INC1.5), and Ti6Al4V + 2.5% IN718 (INC2.5). Samples were all printed with 30 µm layer height, 180 W laser power, 1600 mm/s scanning speed, and 70 µm hatch spacing. Each sample had a 2-3 mm solid support section to cut the parts off with a band saw. Each batch included multiple cylindrical compression samples for testing and large square samples for imaging, microstructural analysis, and Vickers hardness testing. Various part designs were printed, including a lattice gear, model lance, and a ring, to determine if macrocracks would be observed in parts with different features, such as sharp edges, thin features, and large cross sections. Each large square sample was cut in half, mounted in acrylic resin, grinding from 80-2000 grit sandpaper, and polished using a 1 µm colloidal silica suspension. The hardness of each square sample was then measured using a Micro Vickers Hardness Tester (with 0.98N load and 15 sec dwell time) and was then etched for 30s using Kroll's reagent. A field emission scanning electron microscope (FESEM, FEI-SIRION, Portland, OR) was then used to observe the microstructure, followed by Energy Dispersive Spectroscopy (EDS) to see the distribution of elements and highlight inclusions and intermetallic phases in the microstructure. For compression testing, an Instron compression tester was used to test n = 3 different cylindrical samples (8mm diameter by 16mm height) from each contaminated batch, and one sample was tested from the control Ti6Al4V until failure at a speed of 1.3 mm/min.

3. Results and Discussion

The extent of cracking in the printed samples varied in surface-level visibility. Some cracks were very evident, i.e., the square block and some were hidden in the complex shapes such as the model lance (See **Fig. 2A**). All designs produced with a 0.5 wt% contamination amount of IN718 exhibited no visible cracking, indicating that they might pass a visible inspection post-print. However, the increased amounts of contamination, i.e., 1.5 wt% and 2.5 wt%, resulted in cracking due to stress concentration in geometrically complex regions and on flat faces of the lances, blocks, and gears.

Fig. 2B shows the SEM and EDS analysis results of the cross sections. The pure Ti6Al4V sample displays needle-like α' grains throughout the sample, whereas the contaminated samples displayed non-uniformly distributed inclusions throughout the as-built structure. Using EDS, a higher amount of Ni and a lower amount of Ti could be identified as brittle intermetallic phase formations or partially melted IN718 particles in the microstructure. These regions were most evident in the samples produced with 2.5 wt % contamination and were very limited in presence at lower wt % contamination samples. The size of these formations in the 2.5 wt % samples is on the order of the powder particle size (50μm), indicating limited melting of the IN718 powder during printing. However, during printing, the inhomogeneous Ti-elemental distribution within the inclusions points towards a complex elemental diffusion within the melt pool. The scant IN718 particles are swept into the titanium melt, which then begins reacting, forming intermetallic phases and creating a complex state of diffusion that leaves the inhomogeneity. The non-uniform distributions of Ni-Ti intermetallics and voids/porosity were expected, as these had been observed in Ni-Ti bimetallic welds and structures [19-22]. **Fig. 2B** (Bottom) shows a single XRD test performed for the INC2.5 sample where all Ti6Al4V peaks are present, and no additional peaks are observed, indicating that contamination is not influencing the bulk phase evolution of the parts during the printing process.

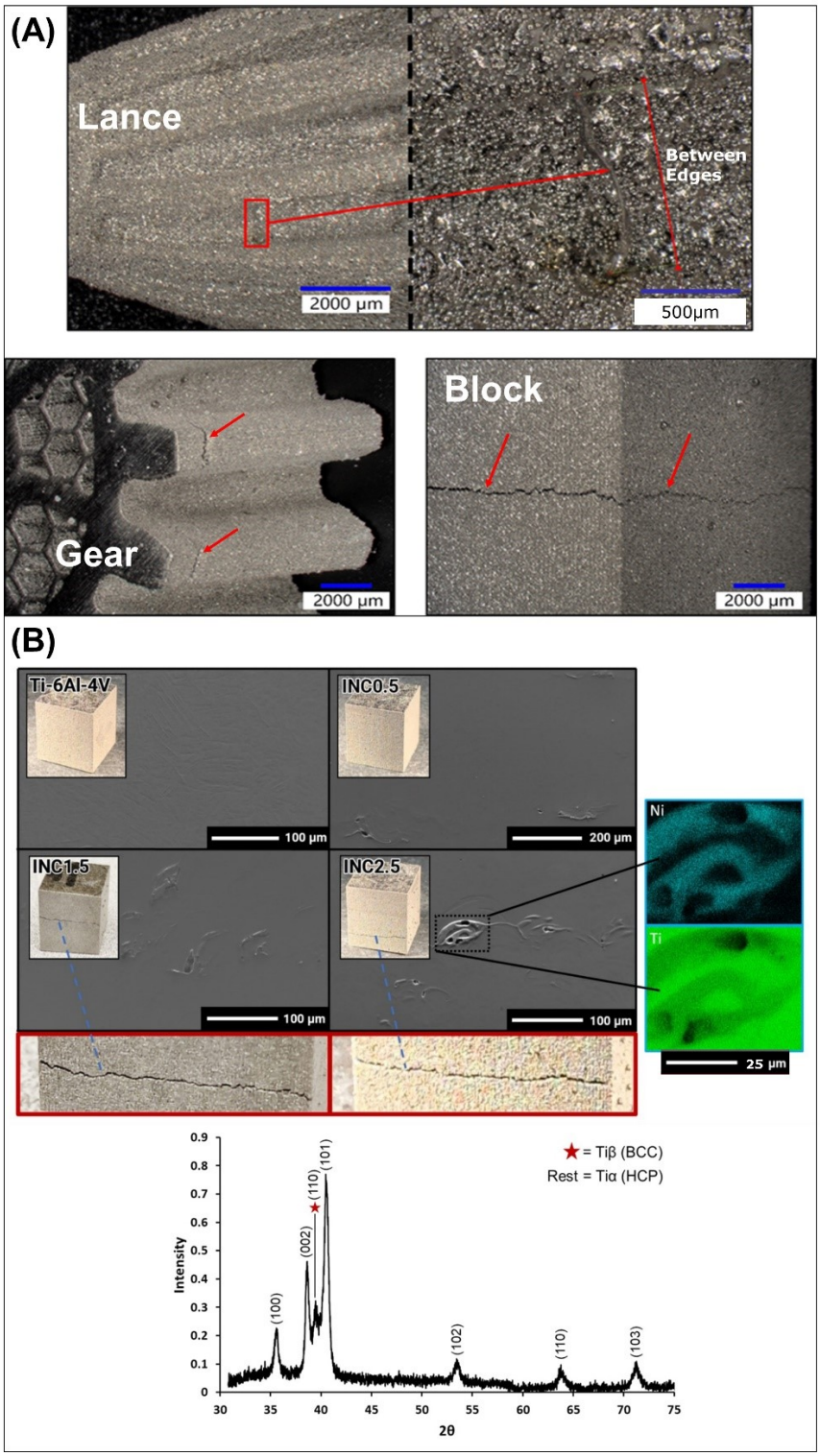

Figure 2: Cracking and defects in contaminated samples. **(A)** Model lance, gear, and block were all produced with > 0.5wt% contamination. The edges of the lance faces are identified in the enhanced image. **(B)** SEM micrographs, EDS analysis, and XRD of contaminated samples show Ni-rich inclusions.

Fig. 3A shows the results of the Vickers hardness testing, which shows increases with increasing contamination content. Ti6Al4V has the lowest average hardness of 386 HV, and INC1.5 has the highest average of 479 HV. The increasing volume fraction of the intermetallic phase in the microstructure contributes to this increased hardness through Orowan strengthening, i.e., the hard intermetallic phase impedes dislocation motion, thereby resisting plastic deformation under a concentrated point loading. The most conceptually significant trend is the standard deviation, starting at ± 6.4 HV in the pure Ti6Al4V sample and peaking in the INC1.5 sample at ± 24.3 HV, which points to variation across the sample due to varying intermetallic phase density. At 2.5 wt% contamination, the material properties approach that of a metal-ceramic composite with highly variable and non-uniform properties compared to a pure metal where the hardness is more uniform.

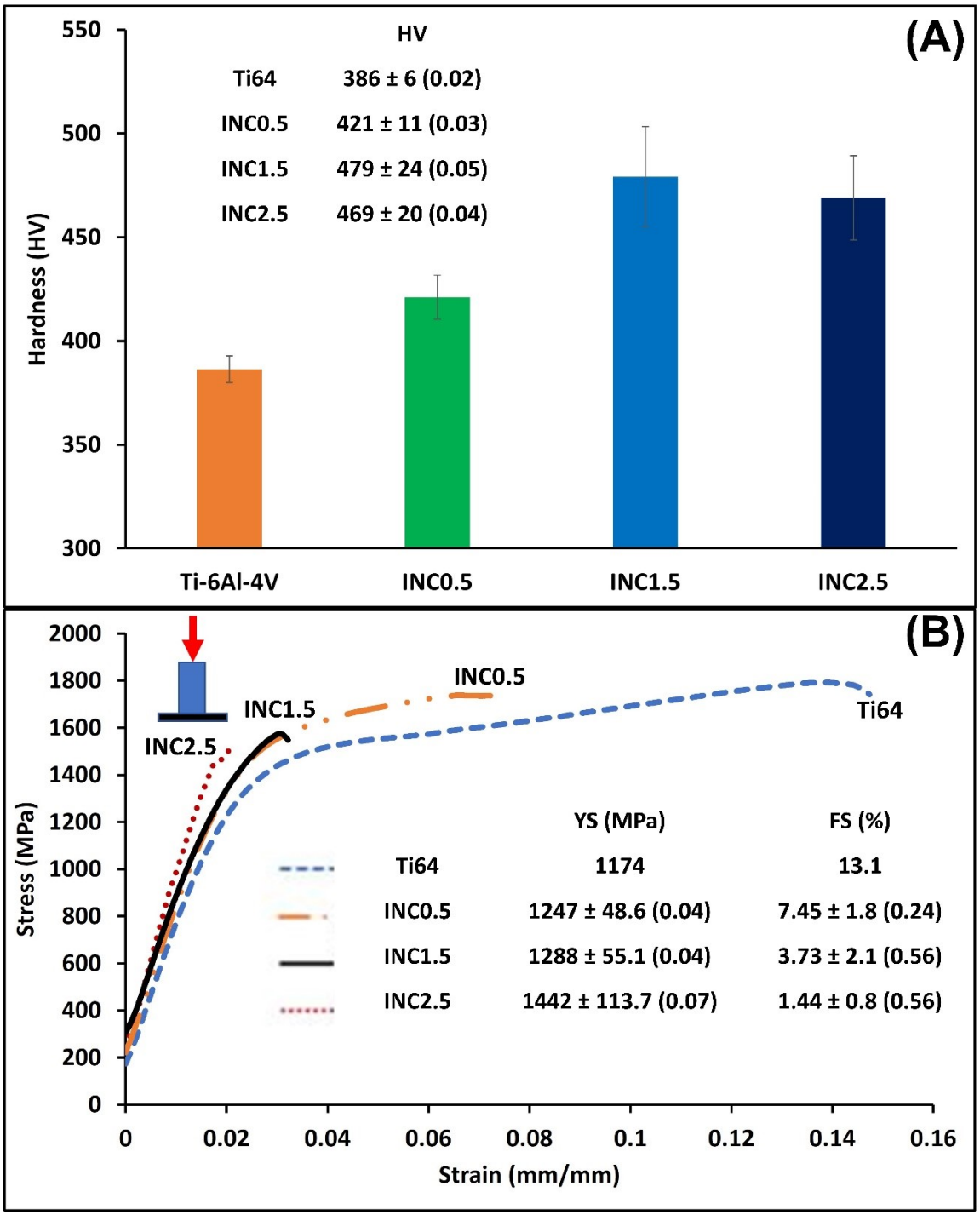

Figure 3: (A) Vickers hardness results for each composition. **(B)** Stress-strain curves for each contaminated batch's lowest plastic strain solid cylindrical samples to pure Ti6Al4V, with tabulated averages for Yield Strength (YS) and Failure Strain (FS). The coefficient of variation of the standard deviation is in parentheses beside each tabulated value.

Fig. 3B shows the stress-strain curves of the pure Ti6Al4V and the lowest-strength performing contamination samples of the three in terms of the amount of plastic region strain. The lowest-strength contamination sample for the INC0.5 composition shows a 55.5% (0.131 strain to 0.0593 strain) decrease in the plastic region strain compared to pure Ti6Al4V. In the worst-case scenario for the INC1.5 and INC2.5 compositions, a plastic region strain of 1.67% and 0.833% were observed. Very high standard deviations for plastic region strain in all the contaminated compositions are evident, while small yield strength standard deviation increases are also observed. Although there is an increase in yield strength with increasing contamination, there is a significant dropoff in plastic strain. This manifests clearly in the IN0.5 sample, which shows no visible contamination yet maintains an average 6.2% increase in yield strength over Ti6Al4V and a 43% reduction in plastic region strain. This effect indicates that the inclusions merely act as a site for crack initiation and propagation under loading, contributing to a more brittle failure mechanism than pure Ti6Al4V.

4. Conclusions

Ti6Al4V parts with variable IN718 contamination content were printed via powder bed fusion (PBF) additive manufacturing. Parts with > 0.5wt% contamination exhibited no visible defects; however, SEM/EDS analysis revealed non-uniform distributions of brittle Ni-Ti intermetallics throughout the samples. A 43% reduction in plastic strain was observed going from pure Ti6Al4V to IN0.5 for the solid cylinders, and even further decreases for higher amounts of contamination. Our results highlight the challenge during a material changeover: no visible signs of cracking can occur in contaminated samples, but it can still significantly degrade mechanical properties.

5. Acknowledgments

The authors would like to acknowledge financial support from the National Science Foundation under Grant Number CMMI 1934230.

6. Declaration of competing interest

The authors declare that they have no known competing interests.

7. References

[1] Onuike et al., *Materials Letters* 252 (2019): 256-259.

[2] Wang et al., *Materials Today* 59 (2022): 133-160.

[3] Dejene et al. *Metals* 13 (2023): 424.

[4] Bandyopadhyay et al., *Materials Today* 52 (2022): 207–224.

[5] Santecchia et al. *Materials* 12 (2019): 2342.

[6] Sanaei et al., *Prog Mater Sci* 117 (2021): 100724.

[7] Kennedy et al. *Journal of Materials Engineering and Performance* 28 (2019): 728–40.

[8] Wu et al., *Additive Manufacturing* 29 (2019): 100808.

[9] Gatto et al. *Additive Manufacturing* 24 (2018): 13–19.

[10] Brandão et al. *Materials* 10, no. 5 (May 2017): 522.

[11] Liu et al. *Materials & Design* 164 (2019): 107552.

[12] Rack et al., *Materials Science and Engineering: C* 26 (2006):1269-1277.

[13] Mitra et al., *Materials Today* 45 (2021): 20-34.

[14] Dietrich et al. *Additive Manufacturing* 32 (2020): 100980.

[15] Hosseini et al. *Additive Manufacturing* 30: 100877.

[16] Moeinfar et al., *Journal of Materials Research and Technology* 16 (2022): 1029–1068.

[17] Tran et al. *Surface and Coatings Technology* 321 (2017): 425–37.

[18] Chen et al. *The International Journal of Advanced Manufacturing Technology* 52, no. 9 (2011): 977–87.

[19] Onuike et al., *Additive Manufacturing* 22 (2018): 844–51.

[20] Afrouzian et al. *Materials & Design* 215 (2022): 110461.

[21] Bandyopadhyay et al., *Virtual and Physical Prototyping* 17 (2022): 256-294.

[22] Ojo et al., *Metall. & Mater. Trans. A* 38 (2007): 356–369.